Molecular Therapy
Nucleic Acids
Original Article

Mechanistic intracellular PK/PD modeling to inform development strategies for small interfering RNA therapeutics

Lin Chen,[1] Caroline Bosmajian,[1] and Sukyung Woo[1]

[1]Division of Pharmacokinetics-Pharmacodynamics and Systems Pharmacology, Department of Pharmaceutical Sciences, School of Pharmacy and Pharmaceutical Sciences, University at Buffalo, The State University of New York, Buffalo, NY 14214, USA

Small interfering RNA (siRNA) therapeutics provide a targeted approach to silence disease-related genes, with notable success in liver-targeting applications. However, the quantitative effects of siRNA properties, such as stability and affinity, as well as biological factors like cell proliferation, mRNA turnover, and abundance, on gene silencing, particularly for extrahepatic targets, remain poorly understood. To identify determinants influencing gene knockdown extent and duration, we developed a mechanistic intracellular pharmacokinetic/pharmacodynamic (PK/PD) model for RNAiMAX-delivered siRNA, based on cytoplasmic siRNA disposition, RISC-loaded siRNA exposure, and mRNA knockdown across different targets in MCF7 and BT474 cells. The model highlighted the critical roles of cell proliferation in silencing duration and mRNA turnover rates on knockdown extent. In rapid-dividing cells, mRNA half-life drives knockdown profiles, whereas chemical siRNA stabilization extends silencing in slow-dividing cells. Targets with extremely low or high mRNA abundance pose silencing challenges. While sufficient RISC occupancy is essential, increasing RISC exposure has minimal impact on silencing extent; enhancing siRNA-mRNA target engagement is more effective. The model also defined a quantitative relationship for maximal mRNA knockdown, governed by cell proliferation, mRNA half-life, and RISC-mediated cleavage rates. This mechanistic PK/PD modeling provides insights into optimizing siRNA design and target selection in therapeutic development.

INTRODUCTION

RNA interference (RNAi) is an endogenous cellular mechanism that regulates gene expression at the post-transcriptional level.[1] By harnessing this intrinsic biologic process, RNAi-based therapeutics, which can theoretically silence any disease-related gene in a sequence-specific manner, are revolutionizing drug development by offering innovative treatments for diverse diseases.[2–4] Small interfering RNAs (siRNAs), a type of noncoding small RNA 20–30 nt in length, can mediate the cleavage of disease-related mRNAs to achieve therapeutic effects.[5,6] In 2018, the US Food and Drug Administration approved the first lipid nanoparticle (LNP)-based siRNA therapy (Onpattro [patisiran]) for the treatment of hereditary amyloidogenic transthyretin amyloidosis with polyneuropathy in adults.[7] Since then, leveraging the specific binding interaction between *N*-acetylgalactosamine (GalNAc) and the asialoglycoprotein receptor (ASGPR), a receptor specifically expressed on the surface of hepatocyte membranes,[8]—five liver-targeting GalNAc-conjugated siRNAs have been approved.[9,10]

From discovery to clinical application, significant efforts have been dedicated to overcoming various obstacles in the field of siRNA therapeutics. For instance, the introduction of chemical modifications at the phosphate backbone (e.g., phosphorothioate), the ribose moiety (e.g., 2′-*O*-methyl), or the base of nucleotides not only prevents systemic siRNA degradation but also enhances siRNA activity and specificity, thereby minimizing off-target effects.[11,12] Furthermore, advances in delivery platforms, such as GalNAc conjugates and LNPs, have facilitated safe and efficient siRNA delivery to specific tissues and cells, ensuring adequate engagement of siRNA and RNA-induced silencing complex (RISC) to cleave target mRNA.[13,14]

A notable feature of siRNA therapeutics is the disconnection between transient systemic exposure and prolonged pharmacological effects. For example, the liver-targeting GalNAc-siRNA Leqvio (inclisiran) has a dosing interval of every 3–6 months, despite exhibiting a short terminal half-life of 5.2 h in human plasma.[10] While siRNA stabilization and administration route have demonstrated significant impacts on the long-term activity of liver-targeting siRNAs,[15] a quantitative understanding of potential other determinants of gene silencing and extrapolating these findings to extrahepatic indications remain a challenge. Conversely, while there has been extensive focus on siRNA properties (e.g., siRNA stability and affinity), the investigation of the influence of biological systems (e.g., cell proliferation) and target characteristics (e.g., mRNA turnover and abundance) on gene silencing has been largely limited.

Received 5 September 2024; accepted 12 March 2025;
https://doi.org/10.1016/j.omtn.2025.102516.

Correspondence: Sukyung Woo, PhD, Professor, Department of Pharmaceutical Sciences, School of Pharmacy & Pharmaceutical Sciences, The State University of New York at Buffalo, 352 Pharmacy Building, Buffalo, NY 14214, USA.
E-mail: skwoo@buffalo.edu

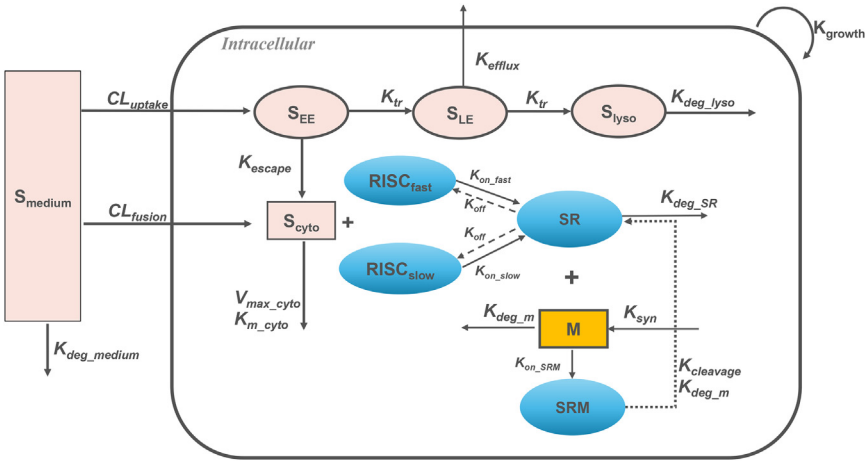

Figure 1. Schematic of the intracellular PK/PD model for liposome-encapsulated siRNA

The model outlines key steps: siRNA uptake via endocytosis (CL_{uptake}) and fusion (CL_{fusion}) from the extracellular medium (S_{medium}), endolysosomal trafficking (K_{tr}), escape from early endosomes (S_{EE}, K_{escape}), exocytosis from late endosomes (S_{LE}, K_{efflux}), lysosomal degradation (S_{lyso}, K_{deg_lyso}), loading of cytosolic free siRNA (S_{cyto}) onto free RISC to form the siRNA-RISC complex (SR, K_{on}, K_{off}), formation of the ternary complex between SR and target mRNA (SRM, K_{on_SRM}), siRNA-mediated mRNA cleavage ($K_{cleavage}$), and siRNA stability in the extracellular medium (K_{deg_medium}) and cytoplasm (V_{max_cyto}, K_{m_cyto}). The RISC loading process occurs in two phases: an initial rapid, small-scale loading (K_{on_fast}, $RISC_{fast}$), followed by a slower, larger-scale loading (K_{on_slow}, $RISC_{slow}$). Target mRNA (M) turnover is described by synthesis (K_{syn}) and degradation (K_{deg_m}). Model parameters are defined in Table 1, and equations are provided in the materials and methods section. Cytoplasmic siRNA represents total intracellular siRNA, while cytosolic siRNA represents siRNA within the intracellular fluid portion.

Mechanistic pharmacokinetic/pharmacodynamic (PK/PD) modeling is a powerful tool for comprehensively characterizing the impact of siRNA characteristics, target mRNA properties, and cellular biology systems on the magnitude and duration of siRNA-mediated gene knockdown.[16–18] A physiologically based PK/PD model has demonstrated the feasibility of translating the *in vivo* PK/PD properties of GalNAc-conjugated siRNA across species.[19] This study underscores the importance of intracellular PK/PD characterization, particularly the temporal profiles of RISC-loaded siRNA, for bridging in *vitro-in vivo* results. Although an elegant mathematical model was proposed to evaluate the effect of cell doubling and siRNA stability on gene silencing, the lack of experiment data supporting their findings rendered the model more theoretical and conceptual.[20] Another group successfully established a model to capture RISC-loaded siRNA profiles; however, their focus remained on siRNA uptake within 24 h, neglecting the influences of cell types and target characteristics.[21]

In this study, we successfully developed and validated a mechanistic intracellular PK/PD model (Figure 1) to elucidate the relationship between cytoplasmic siRNA disposition, RISC-loaded siRNA exposure, and mRNA knockdown across multiple targets in diverse cell lines. Our model enabled a comprehensive evaluation of various factors influencing gene silencing, including siRNA stability, siRNA affinity to RISC and the target, cell proliferation, target abundance, and turnover rates. Most importantly, the model provided insights into the maximum achievable knockdown following siRNA treatment. Through the application of this mechanistic PK/PD model, we gained deeper quantitative insights into how siRNA characteristics and biological systems collectively impact the extent and duration of siRNA-mediated gene silencing. These findings offer valuable guidance for optimizing siRNA design and target selection in the development of effective siRNA therapeutics.

RESULTS

Time profiles of intracellular siRNA, RISC-loaded siRNA, and mRNA knockdown

To characterize intracellular siRNA disposition, including RISC-loaded PK profiles, MCF7 and BT474 cells were treated with three different siRNAs for 24 h across different doses, ranging from 0.03 to 3 nM. These siRNAs include dicer-substrate siRNAs against human hypoxanthine phosphoribosyltransferase 1 (DsiHPRT1), glyceraldehyde 3-phosphate dehydrogenase (DsiGAPDH), and peptidylprolyl *cis-trans* isomerase B (DsiPPIB). The typical siRNA structure is shown in Figure S1 and the sequences are listed in Table S1. The intracellular and RISC-loaded amounts of siRNA were quantified using the validated sensitive stem-loop RT-qPCR (quantitative reverse-transcription PCR) method.[22] The time profile data (Figure 2) were analyzed to obtain PK parameters, including terminal half-life ($t_{1/2}$), peak amount (A_{max}), and area under the siRNA-time curve (AUC) (Table S2). After a 24-h exposure to siRNAs, we observed dose-proportional increases in intracellular siRNA exposure (e.g., A_{max}, AUC) across all targets in both cell lines, indicating linear PK behavior up to the highest dose tested. However, RISC-loaded siRNA exposure displayed a less-than-proportional increase at higher doses in both cell lines, indicating saturation of siRNA RISC loading. The half-lives of RISC-loaded siRNA profiles were generally longer than those of cytoplasmic siRNA at each dosing level. Additionally, both the intracellular and RISC-loaded siRNA profiles in MCF7 exhibited a faster decline compared to those in BT474, likely due to the shorter doubling time of MCF7 cells (40 vs. 70 h).

Transfecting different siRNAs at the same dose produced a <2-fold difference in intracellular exposure in MCF7 cells, while BT474 cell showed greater variability. Notably, with escalating doses of DsiHPRT1, the relative exposure of RISC-loaded siRNA to intracellular siRNA ($AUC_{RISC}/AUC_{intracellular}$) decreased from ~4% to ~0.8% in MCF7 and from ~19% to ~2% in BT474 (Table S2). A

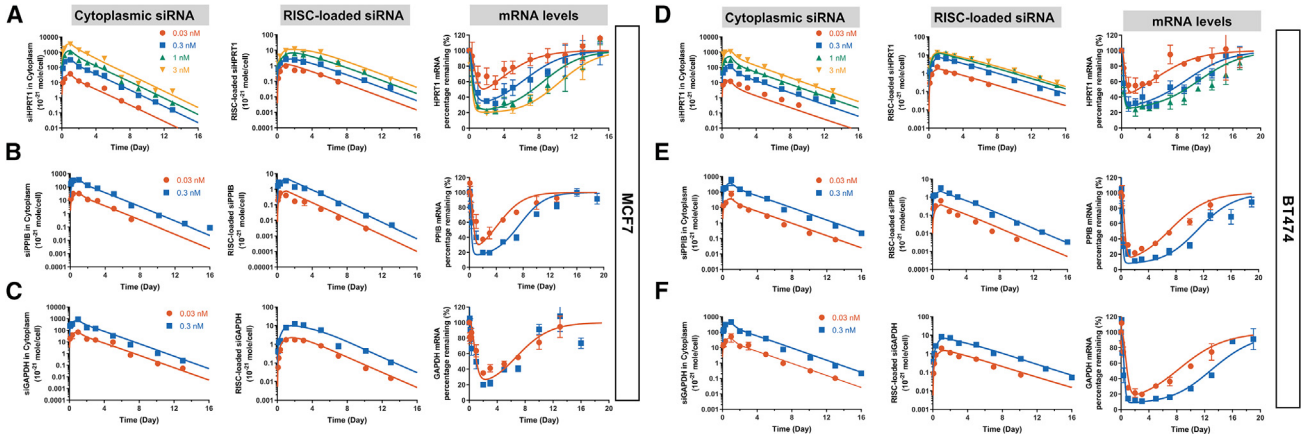

Figure 2. Time profiles of cytoplasmic and RISC-loaded siRNA and mRNA knockdown following *in vitro* treatment with various siRNAs

MCF7 (left) and BT474 (right) cells were treated with siHPRT1 (A and D), siPPIB (B and E), or siGAPDH (C and F) at multiple concentrations (0.03–3 nM), delivered via RNAiMAX. After a 24-h incubation, cells were washed and continued to be cultured in fresh medium. Cells were harvested at specific time points, from 2 h to 19 days since the start of transfection, for quantification of siRNA and mRNA levels. The symbols represent the observed data, while the solid lines represent the model-fitted curves. Data are presented as mean ± SD, with n = 2 for siHPRT1 PK and n = 3 for all other PK/PD data.

similar trend was also observed for the other siRNAs in both cell lines, indicating the limited RISC loading after siRNA cellular delivery at higher doses and a nonlinear RISC loading process.

Compared to total intracellular siRNA profiles, RISC-loaded siRNA profiles were clearly well correlated with the extent and duration of corresponding mRNA knockdown (Figure 2). As RISC-loaded siRNA reached its peak within 24–48 h, maximal gene silencing was also observed during this period, with the knockdown effect lasting longer at higher doses. As siRNA in RISC decreased, mRNA levels gradually returned to their basal state over 16–20 days, with parallel recovery slopes across all dose levels. Notably, following siRNA treatment with the same dose in MCF7 and BT474, a longer recovery time was needed for each target mRNA in BT474 despite similar RISC exposure.

Development of intracellular PK/PD model for siRNAs

We developed an intracellular siRNA PK/PD model (Figure 1; Table 1) to depict the time profiles of intracellular siRNA, RISC-loaded siRNA, and mRNA knockdown for various targets across different doses. Our model incorporates siRNA uptake mechanisms (CL_{uptake}, CL_{fusion}), stability in cytoplasm (V_{max_cyto}, K_{m_cyto}) and extracellular medium (K_{deg_medium}), endosome escape (K_{escape}), exocytosis (K_{efflux}), endolysosomal trafficking (K_{tr}), lysosomal degradation (K_{deg_lyso}), siRNA loading onto RISC (K_{on}, K_{off}), formation of the ternary complex of siRNA-RISC-mRNA (K_{on_SRM}), RISC turnover (K_{deg_SR}), and target mRNA turnover (K_{syn}, K_{deg_m}) and cleavage ($K_{cleavage}$). Several assumptions were made during modeling: (1) the number of cells increase at a linear growth rate (K_{growth}) when appropriate subculturing is applied; (2) apart from endocytosis (CL_{uptake}) for the majority of siRNA cellular uptake, a minor fusion pathway (CL_{fusion}) also contributes to cytosolic siRNA delivery[25]; (3) the RISC loading process involves a two-phase mechanism: an initial rapid, small loading (K_{on_fast}, $RISC_{fast}$), followed by a slower, larger loading (K_{on_slow}, $RISC_{slow}$); (4) once loaded, the dissociation (K_{off}) of siRNA from RISC is negligible[26]; (5) the formation of the siRNA-RISC-mRNA complex (SRM) does not affect the natural degradation of mRNA (K_{deg_m}). Once the mRNA is degraded within the ternary complex, the siRNA-RISC complex (SR) becomes available for another mRNA binding; (6) there is no dissociation of mRNA from SRM. As shown in Figure 2, the model well characterized the time profiles of cytoplasmic siRNA, particularly RISC-loaded siRNA, and the corresponding mRNA knockdown curves for three targets in two cell lines across a wide dose range. The model parameters were estimated with acceptable precision (Table 1).

Cellular uptake and cytoplasmic disposition of siRNA

Fusion-mediated uptake has been shown to be important for cationic lipid-based siRNA delivery and efficient mRNA knockdown.[25] Including this pathway (CL_{fusion}) allowed the model to successfully capture the rapid RISC loading of cytosolic siRNA. Experimentally determined siRNA stability (Figures S2A–S2C) showed nonlinear degradation (V_{max_cyto} and K_{m_cyto}) in the cytoplasm (S_{cyto}) and linear elimination (K_{deg_medium}) in the incubation medium (S_{medium}). For endocytosed siRNA (S_{EE}), only 1% was assumed to escape into the cytoplasm.[23] The model parameters of intracellular trafficking aligned with findings that ∼70% of internalized siRNAs undergo exocytosis/endocytic recycling,[27,28] with the remaining siRNAs primarily trapped in the endolysosomal system.[29] The estimated K_{deg_lyso} (∼0.0091 h^{-1}) was similar across cell lines, suggesting that RNAiMAX encapsulation protects siRNA in lysosomes.

RISC loading and siRNA-mediated mRNA knockdown

The introduction of the two-phase RISC-loading process effectively captured rapid, sufficient siRNA loading at low doses (<10% of

Table 1. Intracellular siRNA PK/PD model parameters

Parameters	Description		MCF7			BT474		
			HPRT1	PPIB	GAPDH	HPRT1	PPIB	GAPDH
Cellular uptake								
CL_{uptake} (pL/h)	cellular uptake by endocytosis		106.2 (9)[a]	111.5 (15)	217.3 (10)	29.88 (8)	119.8 (14)	118.4 (10)
Fusion	MCF7: ratio of CL_{fusion} to CL_{uptake} (F_{fusion})	BT474[b]: maximum siRNA fusion rate: V_{m_fusion} (10^{-21} mol/h)	0.092 (27)			45.28 (13)		
		BT474: siRNA concentration at half of maximum fusion rate: K_{m_fusion} (nM)				0.813 (37)		
Endolysosomal trafficking								
K_{deg_lyso} (h^{-1})	degradation rate constant for lysosomal siRNA		0.906E−2 (2)			0.910E−2 (13)		
K_{tr} (h^{-1})	transit rate constant within endolysosomal system		0.0848 (18)			0.071 (20)		
F_{tr_efflux}	ratio of exocytosis rate to transit rate		1.38 (18)			2.237 (43)		
f_{escape}	fraction of siRNA escape from endosome		0.01[c]					
RISC-siRNA								
$RISC_{tot}$ (10^{-21} mol/cell)	total RISC amount per cell		14.43 (15)			15.20 (8)		
F_r	fraction of fast-loading RISC amount to $RISC_{tot}$		0.094 (20)			0.064 (34)		
K_{on_fast} (nM^{-1} h^{-1})	association rate constant of siRNA to $RISC_{fast}$		0.162 (53)	0.3189 (37)	0.0921 (57)	0.1243 (53)	0.2826 (80)	0.088 (73)
F_{on_slow}	ratio of K_{on_slow} to K_{on_fast}		0.2756E−2 (45)	0.0149 (33)	0.0193 (62)	0.0158 (51)	0.0270 (71)	0.0181 (79)
K_{off}	disassociation rate constant of siRNA from RISC		0.000001					
V_{max_cyto} (10^{-21} mol/h)	maximum degradation rate for siRNA in cytosol		2.765[d]			35.93[d]		
K_{m_cyto} (nM)	cytosolic siRNA concentration at half of maximum degradation rate		19.63 (35)	1.797 (28)	67.81 (36)	56.3 (42)	1.894 (39)	71.08 (50)
K_{deg_SR} (h^{-1})	degradation rate constant of RISC-loaded siRNA		0.3197E−2 (29)	0.9576E−2 (38)	0.2804E−2 (47)	0.3484E−2 (22)	0.9724E−2 (21)	0.4183E−2 (37)
Target mRNA								
K_{on_SRM} (nM^{-1} h^{-1})	association rate constant of RISC-siRNA complex to mRNA		0.1554 (20)	0.4993 (40)	0.0954 (28)	0.3785 (22)	1.965 (45)	0.3257 (39)
$K_{cleavage}$ (h^{-1})	cleavage rate of target mRNA by activated RISC		0.4017 (24)	0.278 (33)	0.3486 (67)	0.3574 (17)	0.3462 (28)	0.3273 (37)
K_{deg_m} (h^{-1})	degradation rate constant for mRNA		0.0544	0.0277	0.0118	0.087	0.0141	0.0118
M_0 (10^{-21} mol/cell)	baseline mRNA amount		0.072	0.177	1.99[e]	0.047	0.091	1.99[e]
Experimental conditions								
K_{ws}	washout parameter to describe the end of incubation		0 during the incubation; 50 after the end of incubation					
K_{growth} (h^{-1})	cell growth rate constant		0.017[f]			0.0099[f]		
K_{deg_medium} (h^{-1})	degradation rate constant of siRNA at medium		0.0232[f]					
V_{cell} (pL)	cell volume		1.76[f]			3.05[f]		
V_{medium} (mL)	volume of incubation medium		0.6[f]					

[a]The values in parentheses represent % coefficient variability (CV).
[b]The fusion pathway in BT474 was described using a nonlinear process.
[c]Based on the literature.[23]
[d]Fixed based on *in vitro* stability assay.
[e]Based on the literature.[24]
[f]Values determined experimentally. K_{escape} and K_{efflux} in Figure 1 are computed as the products of K_{tr} and f_{escape} and K_{tr} and F_{tr_efflux}, respectively.

$RISC_{tot}$) and slow, saturable loading at higher doses. A mechanistic catalytic model linked the RISC-loaded siRNA to mRNA expression.[20,30] siRNA-mRNA binding affinity (*K_{on_SRM}*), leading to the formation of the siRNA-RISC-mRNA ternary complex, represents siRNA target engagement, while the mRNA cleavage rate (*$K_{cleavage}$*) indicates siRNA knockdown efficiency. mRNA turnover rates

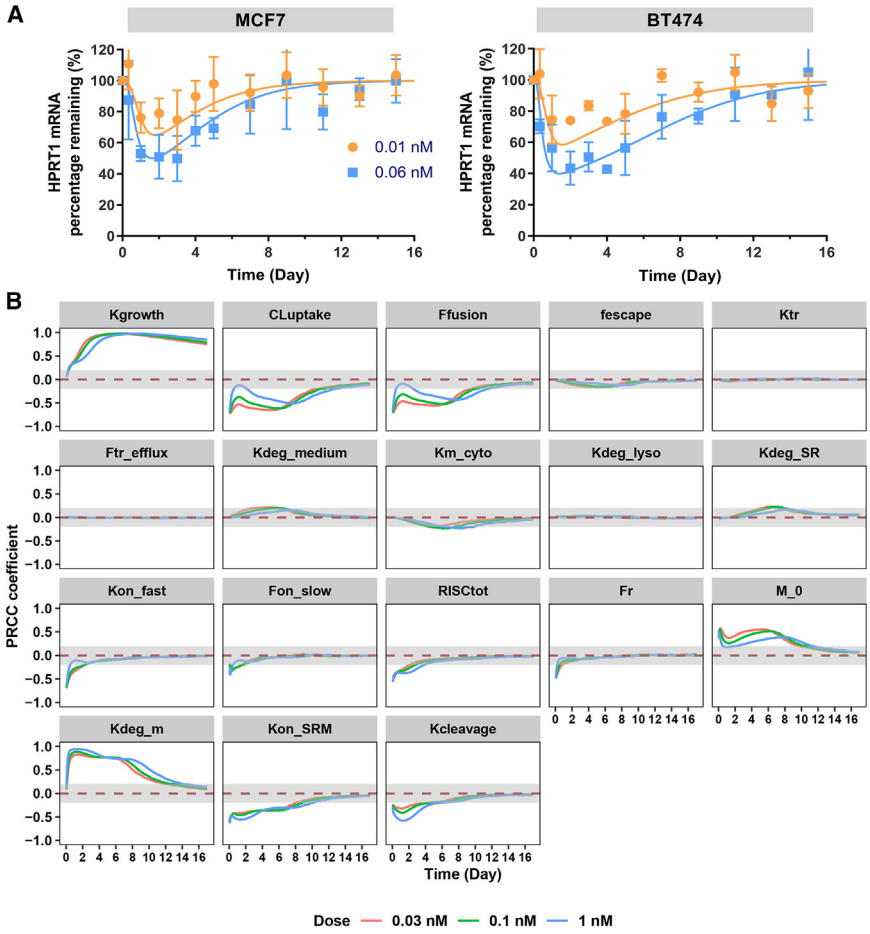

Figure 3. Model validation and global sensitivity analysis

(A) Time profiles of HPRT1 mRNA levels following the treatment with two additional doses of siHPRT1 (0.01 and 0.06 nM) in MCF7 (top left) and BT474 (top right) cells. The model predictions (solid lines) accurately captured the observed mRNA knockdown data (symbols), including the extent and recovery, in both cell lines. The observed data are shown as mean ± SD, with n = 3. (B) PRCC-based GSA results for the intracellular PK/PD model, showing the percentage of remaining mRNA relative to control levels. Definitions of related model parameters are listed in Table 1.

(K_{deg_m}), which were experimentally determined by inhibiting mRNA synthesis,[31] varied across cell lines, with half-lives of 8 vs. 13 h for *HPRT1*, 25 vs. 49 h for *PPIB*, and 59 h for *GAPDH* (Figures S3A–S3C). Our PD model accurately described the slightly delayed onset, extent, and duration of mRNA knockdown (Figure 2). Interestingly, the maximal RISC amount available for siRNA loading ($RISC_{tot}$) was estimated at 15×10^{-21} mol/cell (equivalent to ~9,000 molecules per cell), consistent across cell lines and with the published data.[21,32] It appeared that the same siRNA exhibited different binding affinities to the same target mRNA in distinct cell lines. Surprisingly, the siRNA cleavage rate ($K_{cleavage}$) was consistent (~0.35 h^{-1}) across various targets and cell lines.

Model validation and global sensitivity analysis

We validated our model using HPRT1 mRNA knockdown time profiles at two additional dose levels not included in model development. The model accurately predicted the mRNA knockdown extent and recovery in both cell lines (Figure 3A). Even at low doses (0.01 and 0.06 nM), moderate mRNA knockdown was observed, indicating rapid and sufficient RISC loading of siRNA, further supporting the two-phase RISC loading mechanism. This validation enhances confidence in the model's predictive capability.

We further performed time-variant global sensitivity analysis (GSA) of the PK/PD model for mRNA knockdown (Figure 3B) and siRNA exposure in cytoplasm and RISC (Figures S4A and S4B). The analysis revealed that parameters related to cell and target mRNA characteristics (K_{growth}, M_0, K_{deg_m}) were positively correlated with the remaining mRNA levels. Notably, mRNA half-life (K_{deg_m}) and basal mRNA amount (M_0) significantly affected the onset of mRNA knockdown, while cell doubling time (K_{growth}) and mRNA half-life strongly influenced knockdown duration. As expected, parameters related to siRNA cytosol delivery (CL_{fusion}, F_{fusion}, f_{escape}) were linked to the mRNA knockdown extent, suggesting that enhanced siRNA exposure in the cytosol can lead to more effective knockdown. Surprisingly, siRNA stability parameters (K_{deg_medium}, K_{m_cyto}, K_{deg_SR}) had a relatively minor impact on mRNA knockdown. Additionally, siRNA affinity to RISC and mRNA (K_{on_fast}, F_{on_slow}, K_{on_SRM}) was negatively correlated with remaining mRNA expression, with K_{on_SRM} significantly influencing both the onset and duration of mRNA knockdown.

Effects of cell and target mRNA characteristics on mRNA knockdown

The GSA identified significant effects from cell characteristics, target mRNA, and siRNA properties. To quantitatively assess their influence, comprehensive simulations were performed using key model parameters within ranges based on model estimates and physiologically plausible values (Table S3), while keeping other parameters at reference values. Cell doubling time and mRNA half-life were identified as two most impactful parameters, significantly affecting the extent and duration of mRNA knockdown (Figure 4A). In rapidly dividing cells, a decreased duration of gene silencing was expected due to faster dilution of intracellular siRNA, particularly RISC-loaded siRNA.[20] Knockdown extent was more sensitive to mRNA half-life, with shorter half-lives resulting in less and shorter knockdown, while longer half-lives led to more substantial and prolonged knockdown. This finding

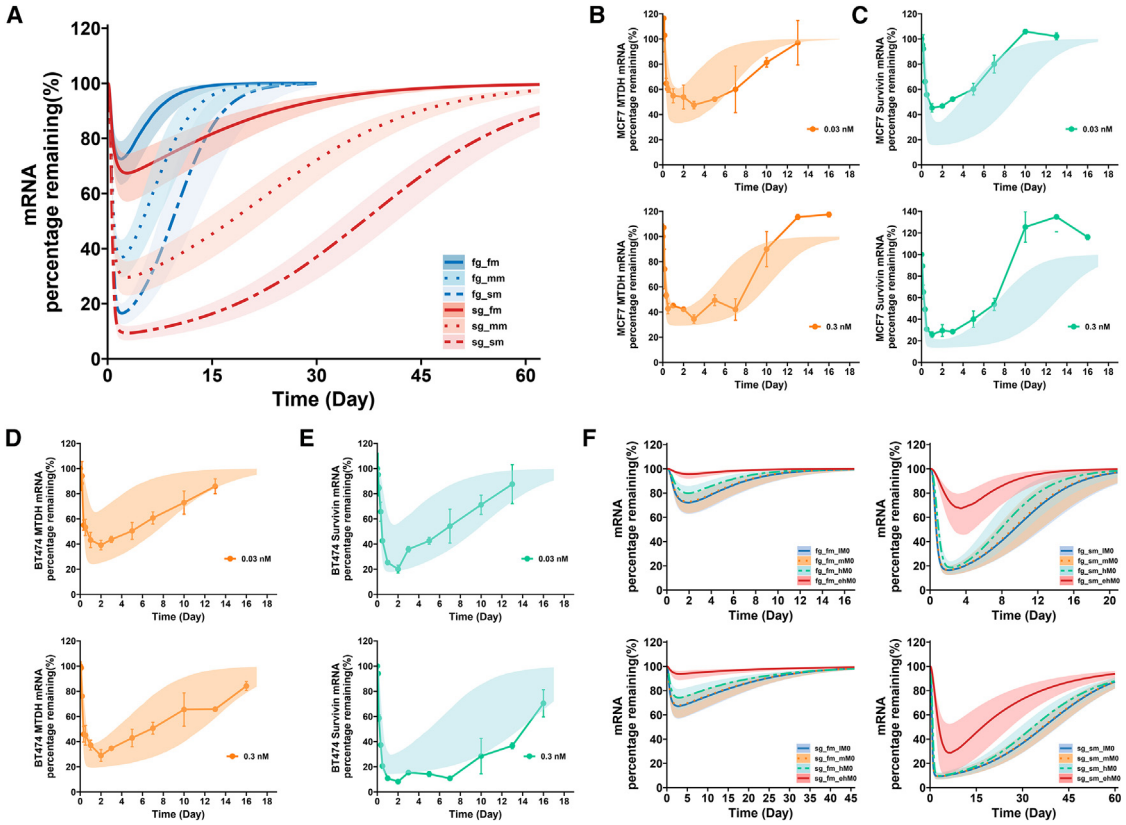

Figure 4. Influence of cell and target mRNA characteristics on gene knockdown

(A) Model-simulated effects of cell proliferation rate and mRNA half-life on knockdown, with cells categorized by fast (fg) and slow (sg) growth rates and mRNAs by fast (fm), medium (mm), and slow (sm) degradation rates. The lines depict the median, and the shaded areas represent the 5th–95th percentiles of 500 simulations. (B–E) Observed and model-predicted time profiles of *MTDH* (B and D) and survivin (C and E) expression after treatment with 0.03 or 0.3 nM siRNA in MCF7 (top) and BT474 (bottom) cells. The shaded areas represent the 5th–95th percentiles of 500 simulations. The observed data (symbols) are shown as mean ± SD, with $n = 2$. (F) Simulated effects of mRNA abundance on knockdown, with expression levels categorized as low (lM0), medium (mM0), high (hM0), and extremely high (ehM0). The lines depict the median, and the shaded areas represent the 5th–95th percentiles of 500 simulations. Parameter values are listed in Table S3.

provides a quantitative explanation for the resistance of mRNAs with short half-lives to siRNA treatment.[33]

To further evaluate the influence of cell doubling time and mRNA half-life, we used two additional targets, metadherin (*MTDH*) and survivin, with half-lives of 8 and 16 h (Figures S3D and S3E), respectively. By focusing on these two parameters and incorporating other model parameter estimates, we simulated mRNA knockdown profiles for both targets at different dosing levels in MCF7 and BT474 cells. Even without specific stability and affinity data for the siRNAs, the model accurately predicted mRNA maximum knockdown and recovery phases for both targets (Figures 4B–4E). These findings emphasize the pivotal roles of cell doubling time and mRNA half-life on siRNA-induced mRNA knockdown and demonstrate the robustness and predictive capability of our model. Additionally, the accelerated recovery of *MTDH* in MCF7 (Figure 4B) and the delayed recovery of survivin in BT474 (Figure 4E) at a higher dose (0.3 nM) may indicate additional complex cellular changes influenced by these oncogenes.

The effect of mRNA abundance on gene knockdown was also assessed (Figure 4F). Independent of cell doubling time and mRNA half-life, mRNA abundance had a negligible impact on knockdown within the range of tens to hundreds of copies per cell (lM0-mM0 groups) and had moderate reduction in the range of several thousand. However, a significant decrease in knockdown was observed for highly overexpressed mRNA (>10,000 copies/cell). Given the abundant target transcripts, limited RISC availability could be the rate-limiting step in cleaving target mRNAs. The simulated competitive and saturable dynamics for high-abundance mRNAs align with the "dilution effect" proposed by Arvey and co-workers,[34] which refers to the phenomenon where the efficiency of silencing decreases due to the abundance of target transcripts. Additionally, mRNAs with longer half-lives appeared less affected by mRNA abundance in terms of knockdown efficiency compared to those with shorter half-lives (Figure 4F). This may present a significant challenge in effectively silencing high-abundance mRNAs to desired levels, particularly for mRNAs with fast turnover rates.

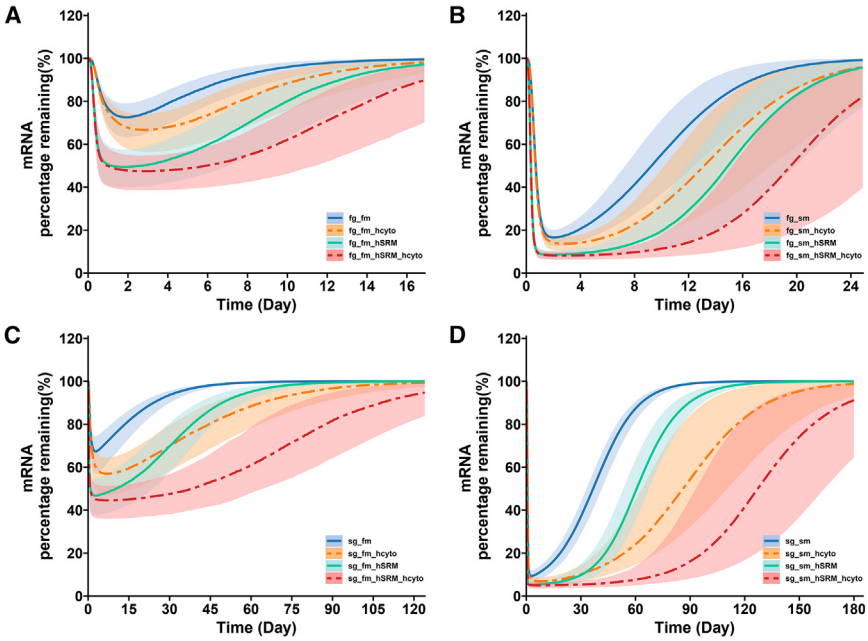

Figure 5. Influence of siRNA stability and target engagement on gene silencing

The effects of siRNA stability and target engagement were assessed in (A) fast-growing cells with short half-life mRNAs (fg_fm), (B) fast-growing cells with long half-life mRNAs (fg_sm), (C) slow-growing cells with short half-life mRNAs (sg_fm), and (D) slow-growing cells with long half-life mRNAs (sg_sm). "hcyto" refers to siRNAs with enhanced cytosolic stability, and "hSRM" indicates enhanced siRNA-mRNA affinity, both compared to reference values. Parameter details are provided in Table S3. The lines represent the median, with the shaded areas indicating the 5th–95th percentiles of 500 simulations.

Effects of siRNA stability and affinity on mRNA knockdown

Enhancing siRNA stability in rapidly dividing cells had limited benefits for mRNAs silencing, regardless of half-life (Figures 5A and 5B). Instead, improving siRNA-mRNA affinity showed a more pronounced impact on both the extent and duration of knockdown. Interestingly, increasing siRNA affinity to RISC, which led to about a 3-fold increase in RISC-loaded siRNA exposure, had only a minor effect on gene silencing (Figures S5A–S5C). Thus, for mRNAs in fast-proliferating cells, enhancing siRNA-mRNA affinity (e.g., target engagement) is more effective than siRNA stabilization. Combining improved siRNA stability and affinity can extend gene silencing from days to weeks in these cells (Figures 5A and 5B).

In contrast, siRNA stabilization had a more pronounced effect in slow-dividing cells (Figures 5C and 5D). For mRNAs with short half-lives, engineering more stable siRNAs could intensify knockdown and extend their duration from 2 weeks to 2 months. When combined with enhanced siRNA-mRNA affinity, which primarily affects knockdown extent, silencing for mRNAs with short half-lives could be prolonged from a few weeks to >3 months (Figure 5C). For long half-life transcripts in slow-dividing cells, siRNA stabilization was comparable to improved affinity in affecting knockdown extent, but it had a greater impact on prolonging duration. Combining these two strategies could extend gene silencing from under 2 months to 6 months (Figure 5D). However, enhancing siRNA affinity to RISC had minimal effects in slow-dividing cells (Figures S5D–S5F).

Prediction of maximum knockdown capacity

Simulations consistently showed that mRNAs with longer half-lives experienced greater knockdown compared to those with shorter half-lives under the same doses and cell lines. We observed a limiting boundary for the maximal achievable knockdown, varying by mRNA half-life (Figure S6). We derived the limiting condition for the minimum remaining relative mRNA expression (RE_{mRNA_min}) after siRNA treatment by rearranging Equations 13, 14, and 15 (Equations S1–S6):

$$RE_{mRNA\_min} = \frac{K_{growth}+K_{deg\_m}}{K_{growth}+K_{deg\_m}+K_{cleavage}} \quad \text{(Equation 1)}$$

This relationship reveals that RE_{mRNA_min}, or maximum knockdown capacity, is determined by cell doubling time (K_{growth}), mRNA half-life (K_{deg_m}), and RISC-mediated mRNA cleavage rate ($K_{cleavege}$), independent of siRNA doses, stability, or affinity. While K_{growth} and K_{deg_m} are system-specific parameters, $K_{cleavage}$ is related to siRNA properties. Notably, the estimated $K_{cleavage}$ remained consistent at around 0.35 h^{-1} across different targets and cell lines, aligning with reported Ago2-mediated mRNA cleavage rates (0.36–1.44 h^{-1}),[30] which suggests that there may be a physiological limit for $K_{cleavage}$.

To validate the model-informed knockdown limit, we tested for five mRNAs used in model establishment (*HPRT1*, *PPIB*, *GAPDH*) and evaluation (*MTDH*, survivin). The observed maximum knockdown for each target (Figure S7) aligned with or fell within the predicted RE_{mRNA_min} boundary as a function of mRNA half-life (Figure 6A). A clear trend was that the shorter the mRNA half-life, the lesser the knockdown extent.

Given the predicted challenge of silencing mRNAs with short half-lives, we further validated the RE_{mRNA_min} formula using three additional short half-life mRNAs: *c-MYC*, *FOXO3*, and *DGKE*, with half-lives of 0.6, 2–5, and 5–6 h, respectively (Figure S8). Testing the three most potent siRNAs for each target at 10 and 30 nM, the observed maximum knockdowns were well within the predicted values (Figure 6B), reaffirming our findings in both MCF7 and BT474, as well

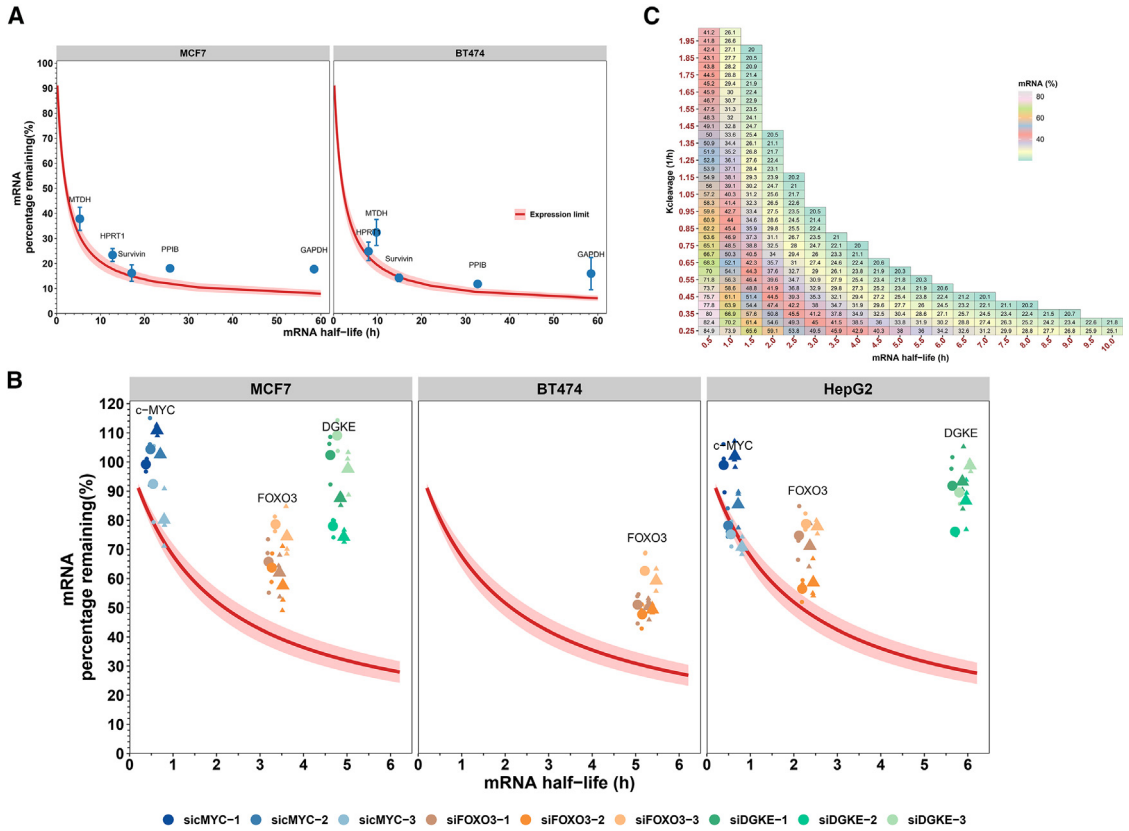

Figure 6. Assessment of model-informed siRNA-mediated maximum knockdown capacity

(A) Comparison of observed versus model-informed maximum knockdown for selected mRNA targets. The points represent the observed maximum knockdown in MCF7 and BT474 cells (Figure S7). The red lines depict the median, with the shaded areas indicating the 5th–95th percentiles of 500 simulations. For simulations, K_{growth} and K_{deg_m} were experimentally determined, and $K_{cleavage}$ was based on model-estimated ranges. (B) Comparison of observed versus predicted maximum knockdown for mRNAs with short half-lives. Cells were treated with siRNAs for 24 h and then collected for mRNA quantification. The small circles and triangles show the observed mRNA levels after 10 and 30 nM siRNA treatments, respectively. The large circles and triangles represent the mean observed levels (n = 3). The red lines depict the median predicted values, and the red shaded areas represent the 5th–95th percentiles of 500 simulations. (C) The predicted minimum remaining mRNA levels (maximum knockdown capacity) across varying $K_{cleavage}$ and mRNA half-lives in cells with a 48-h doubling time. Only remaining mRNA levels above 20% are shown.

as the newly tested HepG2 cells. For mRNAs with short half-lives, enhancing $K_{cleavage}$ appears the most feasible.[35] Our simulations suggested that in fast-growing cells, achieving >80% knockdown with a $K_{cleavage}$ of 0.35 h^{-1} is easier for mRNAs with half-lives >10 h, while significant enhancement in $K_{cleavage}$ is needed for those with half-lives <2 h (Figure 6C).

DISCUSSION

siRNA therapeutics have demonstrated substantial benefits for the treatment of various diseases due to their innovative therapeutic mechanism, high selectivity, and broad applicability.[36,37] However, despite their potential, a comprehensive quantitative understanding of how cell biology (e.g., proliferation), siRNA, and mRNA characteristics influence therapeutic efficacy remains incomplete. To assess the factors of interest, particularly the influence of cell proliferation and mRNA characteristics, we chose to employ the knockdown of housekeeping genes in cancer cells. Given the remarkable adaptability and tolerance exhibited by cancer cells, silencing these housekeeping genes is unlikely to exert a significant impact on their proliferation rates or mRNA characteristics, making them the ideal targets for our evaluation. A mechanistic intracellular PK/PD model was then successfully developed and validated to comprehensively characterize multiple factors, including cell proliferation, siRNA stability, affinity to RISC and mRNA, and target mRNA abundance and turnover rates, on the extent and duration of siRNA-mediated gene silence.

RISC loading of siRNA is the key bioactivation step in the RNAi pathway, closely related to the gene knockdown time course compared to total intracellular exposure.[38,39] Our proposed quantification method determines both single- and double-stranded antisense siRNA in RISC. While a more specific method distinguishing these two species would provide enhanced accuracy for siRNA PK assessment in RISC,[40] quantifying total antisense siRNA in RISC remains a robust approach due to the negligible disassociation of antisense (AS) from RISC and the transient nature of passenger strand cleavage once siRNA is loaded into RISC.[26,41]

Our model proposed a two-phase RISC loading kinetics to characterize this nonlinear process across a wide dosing range (Figures 1 and 2). In contrast, the typical one-phase kinetics either underpredicted RISC exposure at low doses or overestimated it at high doses,[20,21] potentially explaining the underpredicted mRNA knockdown observed at low doses.[19] The two low dosing levels used in our validation further supported the plausibility of the two-phase RISC loading kinetics (Figure 3A). This multi-phase RISC loading process likely arises from competition between exogenous siRNA and endogenous microRNAs (miRNAs) for limited RISC components.[42,43] To achieve RISC occupancy, siRNAs must compete and/or displace RISC-bound miRNAs, which have varying affinities.[44] Additionally, efficient removal of the sense strand impacts RISC accessibility. Ago2 cleaves the sense strand to activate the RISC complex, and inefficient removal can reduce siRNA efficacy.[35] While cellular uptake and trafficking can influence RISC accessibility, they are unlikely to be limiting factors in this study, given the observed linear cellular PK, along with accounted differences between early CL_{fusion} (immediate availability) and steady CL_{uptake} (requiring endosomal escape).

The observed multiphasic kinetics of siRNA-RISC association are more accurately captured by a parallel model structure, which reflects the simultaneous occurrence of different binding states, including weak, transient interactions, intermediate stability complexes, and fully formed, stable RISC complexes. This model accounts for rapid initial binding, followed by slower, more stable complex formation, incorporating factors such as conformational changes in RISC proteins, cooperative effects in assembly, and competition between siRNA molecules for RISC components. Unlike a sequential model, which oversimplifies these interactions, the parallel model captures the coexistence and transitions between multiple binding states, leveraging the high surface area of siRNA for weak complementary interactions.

Our model describes the catalytic nature of RISC-mediated mRNA cleavage, where a single siRNA-loaded RISC can degrade many copies of the target mRNA.[20,30] During model development, we assessed other PD models, such as the stimulation of mRNA degradation (e.g., indirect response model)[45,46] or irreversible inactivation by RISC-loaded siRNA.[47] Although both models adequately described the time course of mRNA, they failed to capture the delay in mRNA knockdown onset. Moreover, these models were insensitive to the effect of initial mRNA abundance.[48]

The effect of mRNA abundance on the mRNA knockdown efficiency of siRNA remains controversial, with reports indicating negative, positive, and no impact.[34,49,50] Considering the total available RISC and the limited number of activated RISC molecules, our model plausibly explains the negligible influence of mRNA abundance ranging from tens to hundreds of copies per cell, with a noticeable negative effect observed for high abundance (e.g., >10,000 copies/cell; Figure 4F). However, for extremely low-abundance mRNAs (<10 copies/cell), efficient target engagement (K_{on_SRM}) is unlikely due to the low probability of mRNA binding to the activated RISC molecules. In such cases, with the reduced K_{on_SRM}, an increase in abundance shows a positive impact on mRNA knockdown. Interestingly, we observed variations in siRNA affinity for its target mRNA across different cell lines. Studies have shown that siRNA efficacy can differ between cell types due to variations in target mRNA abundance, intracellular environment, and mRNA secondary structure. For instance, targeting the same gene (ApoE) resulted in significant efficacy differences between neuronal and astrocytic cell lines.[51] Moreover, siRNAs targeting mRNA regions with unpaired 5′ and 3′ ends exhibited greater silencing, highlighting the importance of target accessibility in gene silencing efficiency.[52]

Our model identified a significant influence of mRNA half-life on mRNA knockdown (Figure 3B). In rapidly dividing cells, mRNA half-life was the key determinant of the knockdown extent and duration (Figures 4B–4E). In such cells, improving siRNA stability showed a limited effect on gene silencing due to the rapid dilution of intracellular siRNA molecules. The shorter knockdown duration (Figures 5A and 5B) aligns with the need for frequent administration of siRNAs in various cancer treatments.[53] Compared to siRNA stabilization, enhancing siRNA-mRNA affinity leads to more pronounced gene silencing in rapidly dividing cells. Strategies to improve mRNA recognition by RISC include appropriate chemical modifications in the siRNA phosphate (e.g., phosphorothioate, phosphorodithioate), ribose (e.g., 2′-*O*-methyl, 2′-*O*-methoxyethyl), and base,[11,54] as well as optimizing the 5′ end of the guide strand, target site accessibility, and the interaction between mRNA structure and RISC.[55–57]

siRNA stabilization significantly impacted gene silencing in slow-dividing cells, particularly for long half-life transcripts (Figures 5C and 5D). Combining siRNA stability and siRNA-mRNA affinity can sustain efficacy for 3–6 months, partly explaining the long dosing intervals of approved siRNA therapies such as Leqvio (inclisiran), which can be administered every 6 months.[10] Interestingly, our simulation showed a minimal effect on gene silencing from increased RISC exposure due to improved siRNA-RISC affinity (Figure S5). This finding is supported by our previous work, which demonstrated a similar extent and duration of mRNA knockdown despite a 10-fold difference in RISC-loaded siRNA exposure.[22] Given the potential off-target effects resulting from the competition and replacement between exogenous siRNA and endogenous miRNA in RISC loading,[42,43,58,59] prioritizing siRNA-mRNA target engagement (K_{on_SRM}) over maximizing siRNA RISC occupancy ($K_{on\_fast/slow}$) is a better design strategy. Therefore, ensuring essential but safe RISC exposure is crucial when considering siRNA delivery strategies. The GalNAc-siRNA conjugate platform, with its extremely slow yet sustained intracellular release of siRNAs, has offered a promising solution.[15] Determining this "therapeutic window" for optimal RISC exposure requires further investigation.

For the first time, our model informed a maximal gene knockdown limit for a given target and cell type after siRNA treatment, which

is determined by the cell doubling time, mRNA half-life, and RISC-mediated cleavage rate (Equation 1). Larsson et al. previously proposed a similar equation, incorporating both endogenous and exogenous factors affecting mRNA decay, to describe changes in mRNA expression.[33] However, their basic model was developed and derived based on mathematical assumptions and could not define what the endogenous and exogenous factors were in detail. Becker et al. derived a more comprehensive equation to predict mRNA steady-state knockdown.[35] Their final equation incorporated mRNA half-life and RISC-mediated cleavage rate, as well as RISC loading-related parameters and additional accelerated mRNA decay rate. Although with rational assumptions, they did not obtain sufficient information on mRNA half-life, accelerated mRNA decay rate, and RISC concentration to support their model application.[35]

Our mechanistic intracellular PK/PD model derived a straightforward yet specific relationship to characterize the maximum mRNA knockdown capacity in siRNA therapeutics. The model was validated with mRNAs with moderate half-lives and three mRNAs with short half-lives, highlighting the challenge of silencing transcripts with very short half-lives. For instance, *c-MYC* achieved only ~20% knockdown, which may partly explain the inefficacy and discontinuation of clinical trials for siRNA targeting this oncogene.[60] *DGKE* also showed less knockdown than predicted despite the moderate turnover rate ($t_{1/2}$ ~5 h), likely due to low mRNA abundance (<5 copies/cell in MCF7 and HepG2 cells), making efficient target engagement difficult. To improve gene silencing of mRNAs with short half-lives, enhancing the $K_{cleavage}$ rate appears to be the most feasible strategy. Despite observing consistent $K_{cleavage}$ values across different targets and cells, this may result from the similar design patterns of the evaluated dicer-substrate siRNAs with high potency. To further evaluate the determinants of $K_{cleavage}$, future studies will incorporate siRNAs with diverse chemical modification patterns. Some studies have observed that specific mismatches between the siRNA guide strand and target mRNAs, as well as the secondary structures of target mRNAs, significantly influence cleavage efficiency.[35,55]

In this study, the utilization of probe siRNAs targeting various mRNAs in cancer cell lines, combined with mechanistic PK/PD modeling, enabled us to identify key factors that determine the extent and duration of gene silencing. Our group will further apply and evaluate these findings both *in vitro* and *in vivo* using clinically relevant hepatic- and extrahepatic-targeting siRNAs. Additionally, the predicted maximum knockdown capacity was only validated with eight targets across three cell lines. Large-scale validation is needed across diverse cell lines and targets, incorporating various siRNA designs and delivery platforms. Table 2 provides a preliminary comparison of RNAiMAX, PEG/lipid nanoparticle, and GalNAc-based siRNA delivery platforms, highlighting anticipated similarities and key differences based on the existing literature and our current understanding. The comparison focuses on key differences likely arising in cellular uptake, endolysosomal trafficking, and escape, with corresponding modifications in model structure and parameters to facilitate its applicability to clinically relevant siRNAs. Due to the limited availability of comprehensive intracellular PK/PD data for PEG/lipid nanoparticles and GalNAc-siRNA platforms, these insights remain qualitative and subject to refinement as more experimental data become available.

In conclusion, this study successfully developed a mechanistic intracellular model for siRNA PK/PD, providing valuable insights into key factors that influence gene silencing, including siRNA stability and affinity, target abundance and turnover rates, and cell proliferation. It underscores the critical role of mRNA half-life, cell doubling time, and RISC-mediated cleavage rates in determining the efficacy and duration of siRNA-mediated knockdown. This model establishes a solid framework for optimizing siRNA design and target selection, thereby advancing the development of siRNA therapeutics.

MATERIALS AND METHODS

Cell lines and siRNAs

The human cancer cell lines of breast MCF7 and BT474 and liver HepG2 were purchased from American Type Culture Collection. The culture medium for MCF7 was minimum essential medium (MEM) containing 10% fetal bovine serum (FBS), 1% penicillin/streptomycin, and 0.01 mg/mL insulin. BT474 cells were grown in Dulbecco's Modified Eagle's Medium (DMEM) with 20% FBS and 1% penicillin/streptomycin. HepG2 cells were cultured in MEM containing 10% FBS and 1% penicillin/streptomycin. Cells were maintained in an incubator at 37°C, 5% CO_2, and 95% humidity.

Dicer-substrate siRNAs (DsiRNAs) against human DsiHPRT1, DsiGAPDH, DsiPPIB, DsiMTDH, survivin, *c-MYC*, *FOXO3*, and *DGKE*, along with a negative control DsiRNA (verified scrambled sequence with no known target), were purchased from Integrated DNA Technologies (IDT) and their sequences are listed in Table S1. Lyophilized siRNAs were reconstituted in IDT Duplex Buffer to a concentration of 100 μM, further diluted to the desired concentrations, and stored at −20°C.

siRNA transfection and gene knockdown

MCF7, BT474, and HepG2 cells were transfected with indicated siRNAs at multiple concentrations using Lipofectamine RNAiMAX (Invitrogen). For instance, in the case of DsiHPRT1, 50,000 MCF7 and 70,000 BT474 cells were seeded in each well of a 24-well plate and allowed to attach overnight. On the second day, cells were exposed to Opti-MEM reduced serum medium (Gibco), which contained either 1 nM negative control DsiRNA or DsiHPRT1 at final concentrations of 0.03, 0.3, 1, and 3 nM. Specifically, the final transfection mixture consisted of 1 μL RNAiMAX per 600 μL Opti-MEM. After a 24-h incubation, cells were washed with PBS and then continued to be cultured in full medium. At specific time points

Table 2. Comparison of intracellular siRNA PK/PD characteristics across delivery platforms

Delivery platform	RNAiMAX	PEG/LNPs	GalNAc conjugation
Cellular uptake mechanisms	• receptor-independent mediated (clathrin- and caveolae-mediated endocytosis and/or micropinocytosis) (CL_{uptake})[61–63] • electrostatic interactions with cell membrane (CL_{fusion})	• receptor-independent mediated (clathrin-mediated endocytosis and/or micropinocytosis)[64,65] • potential fusion	• receptor (ASGPR)-mediated endocytosis[19,66–68]
		• model update: minimal changes necessary	• model update: major changes required for ASGPR-mediated endocytosis processes, with parameters that include $ASGPR_{total}$, binding affinity, internalization, receptor recycling
Endolysosomal trafficking: rate, trigger, extent	• rapid endosomal escape • "bursting effect" of RNAiMAX from positive charge of the lipid[61–63] • electrostatic disruption and fusion from endosomes • ∼1% of siRNA released (f_{escape})[63]	• moderate rate of escape • may vary with liposome materials (e.g., pH-sensitive ionizable lipids that disrupt the endosomal membrane upon protonation[64,65]) • ∼1% of siRNA released	• slow, continuous release • passive escape from endolysosomal pathway • ∼0.1% of siRNA released[69]
		• model update: minimal changes necessary	• model update: minor modifications to account for slow release from acidic endolysosomes/depots, etc.
Efflux/recycling mechanisms	• siRNA that does not escape from endosomes is either trafficked to lysosomes or effluxed from the cell (K_{tr} and F_{tr})	• lipids that do not destabilize endosomes can be recycled to the cell membrane • PEG-lipids and non-escaped RNA may recycle	• ASGPR rapidly recycles back to surface of the cell • fraction of conjugated siRNA may return to cell surface[19,68]
		• model update: minimal changes necessary	• model update: minor changes to account for processes, such as recycling[66]

This summary highlights anticipated similarities and key differences between delivery platforms, along with their implications for model modifications.

between 2 h and 19 days since the start of transfection, cells were harvested by trypsinization and pelleted at 2,000 × *g* for 4 min. The pellets were stored at −80°C until RNA extraction and mRNA determination.

Quantification of cytoplasmic and RISC-loaded siRNA

For cytoplasmic and RISC-loaded siRNA quantification, MCF7 (200,000/well) and BT474 (250,000/well) cells in 6-well plates were transfected as described earlier. At predetermined time points, cells were collected, counted, and processed accordingly for cytoplasmic and RISC-loaded siRNA quantification (approximately 20,000 and 200,000 cells were pelleted, respectively). Our recently developed stem-loop RT-qPCR method alongside immunoprecipitation (IP) was employed for siRNA quantification.[22] For cytoplasmic siRNA extraction, cell pellets were lyzed in 100 µL iScript RT-qPCR sample preparation reagent (Bio-Rad Laboratories), followed by stem-loop RT-qPCR using miR-16 as the endogenous reference for cell number normalization. The TaqMan MicroRNA Reverse Transcription Kit (Thermo Fisher) was used for RT. Briefly, 2 µL cell lysate or standard mixed with 4 µL stem-loop primer mix (250 nM for target siRNA and miR-16) was subject to incubation at 95°C for 5 min, 60°C for 5 min, and held at 4°C. The resulting sample was then combined with 14 µL RT reaction mixture. For qPCR, PowerUp SYBR Green Master Mix (Applied Biosystems) was used in CFX96 RT-PCR (Bio-Rad Laboratories). Thermal cycling conditions comprised 2 min at 50°C, 2 min at 95°C, 40 cycles of 15 s at 95°C, and 1 min at 60°C. Primer sequences for siRNAs are provided in Table S4.

For RISC-loaded siRNA (AS) quantification, cell pellets were lysed in 100 µL IP lysis buffer (Pierce) containing RNaseOUT (1:200, Thermo Fisher) and protease/phosphatase inhibitor cocktail (1:100, Pierce). After incubation and centrifugation, the supernatant (10 µL) was used to determine the total protein concentration using a bicinchoninic acid kit (Pierce) for cell number normalization. Then, the supernatant (85 µL) was incubated with Ago2 antibody (1.3 µg, ab57113, Abcam) at 4°C overnight, followed by mixing with Dynabeads Protein G magnetic beads (20 µL, Life Technologies) at 4°C for an additional 2 h. To release siRNA from Ago2, the magnetic beads were then anchored to the side of the tube using a magnetic bar, washed three times with ice-cold PBS, and incubated with 100 µL iScript reagent at 95°C for 5 min. Finally, the mixture was centrifuged, and the obtained AS was quantified using the stem-loop RT-qPCR method described earlier.[22]

Total RNA extraction and mRNA determination

The E.Z.N.A. HP Total RNA Kit (Omega Biotek) was used for total RNA extraction. The RNA RT process utilized the iScript cDNA Synthesis Kit (Bio-Rad Laboratories), followed by qPCR with the iTaq Universal SYBR Green Kit (Bio-Rad Laboratories) on CFX96 RT-PCR Detection Systems. The thermal reaction program consisted of 3 min at 95°C, 40 cycles of 15 s at 95°C, and 1 min at 60°C. Primers for mRNA targets

were ordered from IDT (sequences in Table S5), with 18s ribosomal RNA as the reference gene. Time-dependent mRNA knockdown, normalized to negative control DsiRNA-treated samples and the endogenous reference gene, was analyzed based on the ΔΔCt method.[70]

mRNA half-life determination

To determine mRNA half-lives, the transcription inhibitor, 5,6-dichloro-1-β-D-ribofuranosylbenzimidazole (DRB, Sigma) was used to block mRNA synthesis.[31] MCF7/BT474 cells (500,000/well) were seeded in 6-well plates with 3 mL culture medium. After cell adhesion, 30 μL of 2 mg/mL DRB was added to achieve a final concentration of 20 μg/mL. Cells were collected at 0, 1, 2, 4, 6, and 8 h post-treatment. Total RNA was extracted, and mRNA levels were determined. Assuming complete transcription shutdown, mRNA decay follows first-order kinetics:[71]

$$\frac{dC_{mRNA}}{dt} = -K_{decay} \times C_{mRNA} \quad \text{(Equation 2)}$$

where C_{mRNA} is mRNA expression and K_{decay} is the decay rate constant. Data fitting (Figure S3) with GraphPad Prism 9 (GraphPad Software) provided mRNA half-lives ($t_{1/2}$) calculated as:

$$t_{1/2} = ln\,2/K_{decay} \quad \text{(Equation 3)}$$

siRNA stability in cytoplasmic extracts and Opti-MEM

Cytoplasmic extracts of MCF7 and BT474 were prepared using NE-PER Nuclear and Cytoplasmic Extraction Reagents (Thermo Scientific) following the manufacturer's instructions. DsiHPRT1 at concentrations ranging from 0.006 to 2 nM (5 μL of stock solution at indicated concentration) was mixed with 95 μL cytoplasmic extracts obtained from 10^6 cells and incubated at 37°C. Samples (5 μL) were collected at 0, 5, 15, and 30 min for siRNA quantification. siRNA degradation in cytoplasmic extracts was concentration dependent (Figures S2A and S2B) and described using a nonlinear equation:

$$\frac{dA_{siRNA}}{dt} = -V_{max} \times C_{siRNA}/(K_m + C_{siRNA}) \quad \text{(Equation 4)}$$

where A_{siRNA} and C_{siRNA} is the siRNA amount and concentration in the incubation system, V_{max} is the maximum degradation rate, and K_m is siRNA concentration at half of V_{max}.

For siRNA stability evaluation in Opti-MEM, RNAiMAX-encapsulated DsiHPRT1 at 1 nM was incubated in 500 μL Opti-MEM at 37°C. Aliquots (10 μL) were collected at 0, 2, 4, 20, and 24 h for siRNA quantification, and DsiHPRT1 degradation followed first-order kinetics (Figure S2C).

Intracellular siRNA PK/PD model development

The differential equations describing the intracellular PK/PD model (Figure 1) are shown as follows and the definitions of model parameters are listed in Table 1.

Cell number (N):

$$\frac{d(N)}{dt} = K_{growth} \times N \quad \text{(Equation 5)}$$

siRNA amount in incubation medium (S_{medium}, 10^{-21} mol):

$$\frac{d(S_{medium})}{dt} = -CL_{uptake} \times S_{medium} / V_{medium} \times N - CL_{fusion} \times S_{medium} / V_{medium} \times N - K_{deg\_medium} \times S_{medium} - K_{ws} \times S_{medium} + F_{tr\_efflux} \times K_{tr} \times S_{LE} \times N \quad \text{(Equation 6)}$$

where $CL_{fusion} = CL_{uptake} \times F_{fusion}$.

siRNA amount in early endosome (S_{EE}, 10^{-21} mol/cell):

$$\frac{d(S_{EE})}{dt} = CL_{uptake} \times S_{medium} / V_{medium} - K_{tr} \times S_{EE} - K_{escape} \times S_{EE} - K_{growth} \times S_{EE} \quad \text{(Equation 7)}$$

where $K_{escape} = f_{escape} \times K_{tr}$.

siRNA amount in late endosome (S_{LE}, 10^{-21} mol/cell):

$$\frac{d(S_{LE})}{dt} = K_{tr} \times S_{EE} - K_{tr} \times S_{LE} - F_{tr\_efflux} \times K_{tr} \times S_{LE} - K_{growth} \times S_{LE} \quad \text{(Equation 8)}$$

siRNA amount in lysosome (S_{lyso}, 10^{-21} mol/cell):

$$\frac{d(S_{lyso})}{dt} = K_{tr} \times S_{LE} - K_{deg\_lyso} \times S_{lyso} - K_{growth} \times S_{lyso} \quad \text{(Equation 9)}$$

Free siRNA amount in cytoplasm (S_{cyto}, 10^{-21} mol/cell):

$$\frac{d(S_{cyto})}{dt} = CL_{fusion} \times S_{medium} / V_{medium} + f_{escape} \times K_{tr} \times S_{EE} - K_{on\_fast} \times S_{cyto} \times (RISC_{fast} - SR_{fast} - SRM_{fast}) / V_{cell} - K_{on\_slow} \times S_{cyto} \times (RISC_{slow} - SR_{slow} - SRM_{slow})/V_{cell} + K_{off} \times SR_{fast} + K_{off} \times SR_{slow} - V_{max\_cyto} \times (S_{cyto} / V_{cell})/(K_{m\_cyto} + S_{cyto} / V_{cell}) - K_{growth} \times S_{cyto} \quad \text{(Equation 10)}$$

where $K_{on\_slow} = K_{on\_fast} \times F_{on\_slow}$; $RISC_{fast} = RISC_{tot} \times F_r$; and $RISC_{slow} = RISC_{tot} - RISC_{fast}$.

siRNA amount loaded into RISC (SR, 10^{-21} mol/cell):

$$\frac{d(SR_{fast})}{dt} = K_{on\_fast} \times S_{cyto} \times (RISC_{fast} - SR_{fast} - SRM_{fast}) / V_{cell} - K_{off} \times SR_{fast} - K_{deg\_SR} \times SR_{fast} - K_{on\_SRM} \times (SR_{fast} - SRM_{fast}) \times M / V_{cell} + (K_{cleavage} + K_{deg\_m}) \times SRM_{fast} - K_{growth} \times SR_{fast} \quad \text{(Equation 11)}$$

$$\frac{d(SR_{slow})}{dt} = K_{on\_slow} \times S_{cyto} \times (RISC_{slow} - SR_{slow} - SRM_{slow}) / V_{cell} - K_{off} \times SR_{slow} - K_{deg\_SR} \times SR_{slow} - K_{on\_SRM} \times (SR_{slow} - SRM_{slow}) \times M / V_{cell} + (K_{cleavage} + K_{deg\_m}) \times SRM_{slow} - K_{growth} \times SR_{slow} \quad \text{(Equation 12)}$$

Formation of siRNA-RISC-mRNA ternary complex (SRM, 10^{-21} mol/cell):

$$\frac{d(SRM_{fast})}{dt} = K_{on\_SRM} \times (SR_{fast} - SRM_{fast}) \times M / V_{cell} - (K_{cleavage} + K_{deg\_m}) \times SRM_{fast} - K_{growth} \times SRM_{fast} \quad \text{(Equation 13)}$$

$$\frac{d(SRM_{slow})}{dt} = K_{on\_SRM} \times (SR_{slow} - SRM_{slow}) \times M / V_{cell} - (K_{cleavage} + K_{deg\_m}) \times SRM_{slow} - K_{growth} \times SRM_{slow} \quad \text{(Equation 14)}$$

Free mRNA amount (M, 10^{-21} mol/cell):

$$\frac{d(M)}{dt} = K_{syn} - (K_{deg\_m} + K_{growth}) \times M - K_{on\_SRM} \times (SR_{fast} - SRM_{fast}) \times M / V_{cell} - K_{on\_SRM} \times (SR_{slow} - SRM_{slow}) \times M / V_{cell} \quad \text{(Equation 15)}$$

The relative mRNA expression (RE_{mRNA}) represents as:

$$RE_{mRNA} = (M + SRM_{fast} + SRM_{slow}) / M_0 \quad \text{(Equation 16)}$$

The model was fitted to the obtained siRNA PK data and mRNA PD data across multiple dosing levels. In the same cell line, apart from the cell biological process, by assuming that different siRNAs share the fusion-mediated uptake, degradation rate in lysosome (K_{deg_lyso}), available total RISC amount ($RISC_{tot}$), and fraction of fast-loading RISC (F_r), the intracellular model was fitted simultaneously to PK/PD data of three different targets. The baseline amount of GAPDH mRNA in MCF7 and BT474 cells was assumed to be 1,200 copies/cell,[24] and copy numbers for the other targets were estimated based on Ct value differences in RT-qPCR analysis. Several parameters were fixed based on the physiological values and experimental determinations (e.g., cell doubling time, mRNA turnover). Time profile of GAPDH mRNA knockdown in 0.3 nM dose group was not included in model fitting because of the unexpected acceleration in mRNA recovery.

Model implementation and simulation

Model fitting was performed using the maximum likelihood method in ADAPT 5 (Biomedical Simulations Resource). A power model was used to represent the variance:

$$V_i = \sigma^2 \times Y_i^{\gamma} \quad \text{(Equation 17)}$$

where V_i is the variance of the ith observation, Y_i is the ith model output, σ is the scaling factor, and γ is the power term for the variance. Goodness-of-fit and model structure selection were assessed by visual inspection, the log likelihood objective function (−2LL), and the precision (coefficient variability %) of estimated parameters. Descriptive PK parameters were calculated using Phoenix WinNonlin (version 8.3, Pharsight) from the mean time profiles of cytoplasmic and RISC-loaded siRNA. Simulations were conducted using Berkeley Madonna (version 8.3.23, University of California, Berkeley) and the R package mrgsolve.[72] Observed and model-predicted PK/PD data were graphed using GraphPad Prism 9 and R (http://www.r-project.org).

GSA

GSA is a powerful tool for identifying which parameters and processes significantly contribute to the overall system outcome.[73] Given the complexity of our model, we implemented a partial rank correlation coefficient (PRCC) method-based GSA in R, simultaneously varying 18 model parameters with a sampling size of 5,000.[19,74] The parameter ranges in the simulation were based on the estimates of different targets and physiologically reasonable values. The ranges of each parameter are listed in Table S6. A positive or negative PRCC coefficient indicates the corresponding positive or negative correlation between the input parameter and the simulated output over time.

DATA AND CODE AVAILABILITY

The data and codes that support the findings of this study are available upon reasonable request from the corresponding author, Sukyung Woo.

ACKNOWLEDGMENTS

This work was supported in part by the Center for Protein Therapeutics at the University at Buffalo, NIH R01CA258546, and funding provided (to S.W.) by the Department of Pharmaceutical Sciences, University at Buffalo.

AUTHOR CONTRIBUTIONS

L.C. and C.B. designed the study, and L.C. conducted the experiments and acquired, analyzed, and interpreted the data. S.W. provided funding, resources, and supervision. L.C., C.B., and S.W. discussed the data. L.C. wrote the manuscript and C.B. and S.W. edited and reviewed the manuscript. All authors read and approved the final manuscript.

DECLARATION OF INTERESTS

The authors declare no competing interests.

SUPPLEMENTAL INFORMATION

Supplemental information can be found online at https://doi.org/10.1016/j.omtn.2025.102516.

REFERENCES

1. Wilson, R.C., and Doudna, J.A. (2013). Molecular mechanisms of RNA interference. Annu. Rev. Biophys. *42*, 217–239.
2. Park, J., Park, J., Pei, Y., Xu, J., and Yeo, Y. (2016). Pharmacokinetics and biodistribution of recently-developed siRNA nanomedicines. Adv. Drug Deliv. Rev. *104*, 93–109.
3. Traber, G.M., and Yu, A.M. (2023). RNAi-Based Therapeutics and Novel RNA Bioengineering Technologies. J. Pharmacol. Exp. Therapeut. *384*, 133–154.
4. Won Lee, J., Kyu Shim, M., Kim, H., Jang, H., Lee, Y., and Hwa Kim, S. (2023). RNAi therapies: Expanding applications for extrahepatic diseases and overcoming delivery challenges. Adv. Drug Deliv. Rev. *201*, 115073.
5. Carthew, R.W., and Sontheimer, E.J. (2009). Origins and Mechanisms of miRNAs and siRNAs. Cell *136*, 642–655.
6. Friedrich, M., and Aigner, A. (2022). Therapeutic siRNA: State-of-the-Art and Future Perspectives. BioDrugs *36*, 549–571.
7. Weng, Y., Xiao, H., Zhang, J., Liang, X.J., and Huang, Y. (2019). RNAi therapeutic and its innovative biotechnological evolution. Biotechnol. Adv. *37*, 801–825.
8. Khorev, O., Stokmaier, D., Schwardt, O., Cutting, B., and Ernst, B. (2008). Trivalent, Gal/GalNAc-containing ligands designed for the asialoglycoprotein receptor. Bioorg. Med. Chem. *16*, 5216–5231.
9. Syed, Y.Y. (2023). Nedosiran: First Approval. Drugs *83*, 1729–1733.
10. Jing, X., Arya, V., Reynolds, K.S., and Rogers, H. (2023). Clinical Pharmacology of RNA Interference-Based Therapeutics: A Summary Based on Food and Drug Administration-Approved Small Interfering RNAs. Drug Metab. Dispos. *51*, 193–198.
11. Hu, B., Zhong, L., Weng, Y., Peng, L., Huang, Y., Zhao, Y., and Liang, X.J. (2020). Therapeutic siRNA: state of the art. Signal Transduct. Targeted Ther. *5*, 101.
12. Raja, M.A.G., Katas, H., and Amjad, M.W. (2019). Design, mechanism, delivery and therapeutics of canonical and Dicer-substrate siRNA. Asian J. Pharm. Sci. *14*, 497–510.
13. Dowdy, S.F. (2017). Overcoming cellular barriers for RNA therapeutics. Nat. Biotechnol. *35*, 222–229.
14. Subhan, M.A., and Torchilin, V.P. (2020). siRNA based drug design, quality, delivery and clinical translation. Nanomedicine. *29*, 102239.
15. Brown, C.R., Gupta, S., Qin, J., Racie, T., He, G., Lentini, S., Malone, R., Yu, M., Matsuda, S., Shulga-Morskaya, S., et al. (2020). Investigating the pharmacodynamic durability of GalNAc-siRNA conjugates. Nucleic Acids Res. *48*, 11827–11844.
16. Mager, D.E., and Jusko, W.J. (2008). Development of translational pharmacokinetic-pharmacodynamic models. Clin. Pharmacol. Ther. *83*, 909–912.
17. Ayyar, V.S., and Jusko, W.J. (2020). Transitioning from Basic toward Systems Pharmacodynamic Models: Lessons from Corticosteroids. Pharmacol. Rev. *72*, 414–438.
18. Jeon, J.Y., Ayyar, V.S., and Mitra, A. (2022). Pharmacokinetic and Pharmacodynamic Modeling of siRNA Therapeutics - a Minireview. Pharm. Res. *39*, 1749–1759.
19. Ayyar, V.S., Song, D., Zheng, S., Carpenter, T., and Heald, D.L. (2021). Minimal Physiologically Based Pharmacokinetic-Pharmacodynamic (mPBPK-PD) Model of N-Acetylgalactosamine-Conjugated Small Interfering RNA Disposition and Gene Silencing in Preclinical Species and Humans. J. Pharmacol. Exp. Therapeut. *379*, 134–146.
20. Bartlett, D.W., and Davis, M.E. (2006). Insights into the kinetics of siRNA-mediated gene silencing from live-cell and live-animal bioluminescent imaging. Nucleic Acids Res. *34*, 322–333.
21. Mihaila, R., Ruhela, D., Keough, E., Cherkaev, E., Chang, S., Galinski, B., Bartz, R., Brown, D., Howell, B., and Cunningham, J.J. (2017). Mathematical Modeling: A Tool for Optimization of Lipid Nanoparticle-Mediated Delivery of siRNA. Mol. Ther. Nucleic Acids *7*, 246–255.
22. Chen, L., Bosmajian, C., and Woo, S. (2024). A highly sensitive stem-loop RT-qPCR method to study siRNA intracellular pharmacokinetics and pharmacodynamics. Biol. Methods Protoc. *9*, bpae029.
23. Gilleron, J., Querbes, W., Zeigerer, A., Borodovsky, A., Marsico, G., Schubert, U., Manygoats, K., Seifert, S., Andree, C., Stöter, M., et al. (2013). Image-based analysis of lipid nanoparticle-mediated siRNA delivery, intracellular trafficking and endosomal escape. Nat. Biotechnol. *31*, 638–646.
24. White, A.K., VanInsberghe, M., Petriv, O.I., Hamidi, M., Sikorski, D., Marra, M.A., Piret, J., Aparicio, S., and Hansen, C.L. (2011). High-throughput microfluidic single-cell RT-qPCR. Proc. Natl. Acad. Sci. USA *108*, 13999–14004.
25. Lu, J.J., Langer, R., and Chen, J. (2009). A novel mechanism is involved in cationic lipid-mediated functional siRNA delivery. Mol. Pharm. *6*, 763–771.
26. De, N., Young, L., Lau, P.W., Meisner, N.C., Morrissey, D.V., and MacRae, I.J. (2013). Highly complementary target RNAs promote release of guide RNAs from human Argonaute2. Mol. Cell *50*, 344–355.
27. Buratta, S., Tancini, B., Sagini, K., Delo, F., Chiaradia, E., Urbanelli, L., and Emiliani, C. (2020). Lysosomal Exocytosis, Exosome Release and Secretory Autophagy: The Autophagic- and Endo-Lysosomal Systems Go Extracellular. Int. J. Mol. Sci. *21*, 2576.
28. Sahay, G., Querbes, W., Alabi, C., Eltoukhy, A., Sarkar, S., Zurenko, C., Karagiannis, E., Love, K., Chen, D., Zoncu, R., et al. (2013). Efficiency of siRNA delivery by lipid nanoparticles is limited by endocytic recycling. Nat. Biotechnol. *31*, 653–658.
29. Wittrup, A., Ai, A., Liu, X., Hamar, P., Trifonova, R., Charisse, K., Manoharan, M., Kirchhausen, T., and Lieberman, J. (2015). Visualizing lipid-formulated siRNA release from endosomes and target gene knockdown. Nat. Biotechnol. *33*, 870–876.
30. Deerberg, A., Willkomm, S., and Restle, T. (2013). Minimal mechanistic model of siRNA-dependent target RNA slicing by recombinant human Argonaute 2 protein. Proc. Natl. Acad. Sci. USA *110*, 17850–17855.
31. Bensaude, O. (2011). Inhibiting eukaryotic transcription: Which compound to choose? How to evaluate its activity? Transcription *2*, 103–108.
32. Mihaila, R., Ruhela, D., Galinski, B., Card, A., Cancilla, M., Shadel, T., Kang, J., Tep, S., Wei, J., Haas, R.M., et al. (2019). Modeling the Kinetics of Lipid-Nanoparticle-Mediated Delivery of Multiple siRNAs to Evaluate the Effect on Competition for Ago2. Mol. Ther. Nucleic Acids *16*, 367–377.
33. Larsson, E., Sander, C., and Marks, D. (2010). mRNA turnover rate limits siRNA and microRNA efficacy. Mol. Syst. Biol. *6*, 433.
34. Arvey, A., Larsson, E., Sander, C., Leslie, C.S., and Marks, D.S. (2010). Target mRNA abundance dilutes microRNA and siRNA activity. Mol. Syst. Biol. *6*, 363.
35. Becker, W.R., Ober-Reynolds, B., Jouravleva, K., Jolly, S.M., Zamore, P.D., and Greenleaf, W.J. (2019). High-Throughput Analysis Reveals Rules for Target RNA Binding and Cleavage by AGO2. Mol. Cell *75*, 741–755.e11.
36. Ranasinghe, P., Addison, M.L., Dear, J.W., and Webb, D.J. (2023). Small interfering RNA: Discovery, pharmacology and clinical development-An introductory review. Br. J. Pharmacol. *180*, 2697–2720.
37. Kara, G., Calin, G.A., and Ozpolat, B. (2022). RNAi-based therapeutics and tumor targeted delivery in cancer. Adv. Drug Deliv. Rev. *182*, 114113.
38. Wei, J., Jones, J., Kang, J., Card, A., Krimm, M., Hancock, P., Pei, Y., Ason, B., Payson, E., Dubinina, N., et al. (2011). RNA-induced silencing complex-bound small interfering RNA is a determinant of RNA interference-mediated gene silencing in mice. Mol. Pharmacol. *79*, 953–963.
39. Nair, J.K., Attarwala, H., Sehgal, A., Wang, Q., Aluri, K., Zhang, X., Gao, M., Liu, J., Indrakanti, R., Schofield, S., et al. (2017). Impact of enhanced metabolic stability on pharmacokinetics and pharmacodynamics of GalNAc-siRNA conjugates. Nucleic Acids Res. *45*, 10969–10977.
40. Xu, R., Njumbe Ediage, E., Verhaeghe, T., Snoeys, J., and Dillen, L. (2024). Therapeutic siRNA Loaded to RISC as Single and Double Strands Requires an Appropriate Quantitative Assay for RISC PK Assessment. Nucleic Acid Therapeut. *34*, 199–210.

41. Matranga, C., Tomari, Y., Shin, C., Bartel, D.P., and Zamore, P.D. (2005). Passenger-strand cleavage facilitates assembly of siRNA into Ago2-containing RNAi enzyme complexes. Cell *123*, 607–620.

42. Khan, A.A., Betel, D., Miller, M.L., Sander, C., Leslie, C.S., and Marks, D.S. (2009). Transfection of small RNAs globally perturbs gene regulation by endogenous microRNAs. Nat. Biotechnol. *27*, 549–555.

43. Liang, X.H., Hart, C.E., and Crooke, S.T. (2013). Transfection of siRNAs can alter miRNA levels and trigger non-specific protein degradation in mammalian cells. Biochim. Biophys. Acta *1829*, 455–468.

44. Flores, O., Kennedy, E.M., Skalsky, R.L., and Cullen, B.R. (2014). Differential RISC association of endogenous human microRNAs predicts their inhibitory potential. Nucleic Acids Res. *42*, 4629–4639.

45. Dayneka, N.L., Garg, V., and Jusko, W.J. (1993). Comparison of four basic models of indirect pharmacodynamic responses. J. Pharmacokinet. Biopharm. *21*, 457–478.

46. Sharma, A., and Jusko, W.J. (1998). Characteristics of indirect pharmacodynamic models and applications to clinical drug responses. Br. J. Clin. Pharmacol. *45*, 229–239.

47. Wang, A.F., and Ayyar, V.S. (2024). Pharmacodynamic Models of Indirect Effects and Irreversible Inactivation with Turnover: Applicability to Mechanism-Based Modeling of Gene Silencing and Targeted Protein Degradation. J. Pharmaceut. Sci. *113*, 191–201.

48. Woo, S., Pawaskar, D., and Jusko, W.J. (2009). Methods of utilizing baseline values for indirect response models. J. Pharmacokinet. Pharmacodyn. *36*, 381–405.

49. Hong, S.W., Jiang, Y., Kim, S., Li, C.J., and Lee, D.K. (2014). Target gene abundance contributes to the efficiency of siRNA-mediated gene silencing. Nucleic Acid Therapeut. *24*, 192–198.

50. Krueger, U., Bergauer, T., Kaufmann, B., Wolter, I., Pilk, S., Heider-Fabian, M., Kirch, S., Artz-Oppitz, C., Isselhorst, M., and Konrad, J. (2007). Insights into effective RNAi gained from large-scale siRNA validation screening. Oligonucleotides *17*, 237–250.

51. Ferguson, C.M., Echeverria, D., Hassler, M., Ly, S., and Khvorova, A. (2020). Cell Type Impacts Accessibility of mRNA to Silencing by RNA Interference. Mol. Ther. Nucleic Acids *21*, 384–393.

52. Gredell, J.A., Berger, A.K., and Walton, S.P. (2008). Impact of target mRNA structure on siRNA silencing efficiency: A large-scale study. Biotechnol. Bioeng. *100*, 744–755.

53. Hattab, D., Gazzali, A.M., and Bakhtiar, A. (2021). Clinical Advances of siRNA-Based Nanotherapeutics for Cancer Treatment. Pharmaceutics *13*, 1009.

54. Khvorova, A., and Watts, J.K. (2017). The chemical evolution of oligonucleotide therapies of clinical utility. Nat. Biotechnol. *35*, 238–248.

55. Ameres, S.L., Martinez, J., and Schroeder, R. (2007). Molecular basis for target RNA recognition and cleavage by human RISC. Cell *130*, 101–112.

56. Zhu, L., Jiang, H., Cao, S., Unarta, I.C., Gao, X., and Huang, X. (2021). Critical role of backbone coordination in the mRNA recognition by RNA induced silencing complex. Commun. Biol. *4*, 1345.

57. Shinohara, F., Oashi, T., Harumoto, T., Nishikawa, T., Takayama, Y., Miyagi, H., Takahashi, Y., Nakajima, T., Sawada, T., Koda, Y., et al. (2021). siRNA potency enhancement via chemical modifications of nucleotide bases at the 5'-end of the siRNA guide strand. RNA *27*, 163–173.

58. Loinger, A., Shemla, Y., Simon, I., Margalit, H., and Biham, O. (2012). Competition between small RNAs: a quantitative view. Biophys. J. *102*, 1712–1721.

59. Koller, E., Propp, S., Murray, H., Lima, W., Bhat, B., Prakash, T.P., Allerson, C.R., Swayze, E.E., Marcusson, E.G., and Dean, N.M. (2006). Competition for RISC binding predicts in vitro potency of siRNA. Nucleic Acids Res. *34*, 4467–4476.

60. Habib, S., Ariatti, M., and Singh, M. (2020). Anti-c-myc RNAi-Based Onconanotherapeutics. Biomedicines *8*, 612.

61. Cardarelli, F., Digiacomo, L., Marchini, C., Amici, A., Salomone, F., Fiume, G., Rossetta, A., Gratton, E., Pozzi, D., and Caracciolo, G. (2016). The intracellular trafficking mechanism of Lipofectamine-based transfection reagents and its implication for gene delivery. Sci. Rep. *6*, 25879.

62. Chatterjee, S., Kon, E., Sharma, P., and Peer, D. (2024). Endosomal escape: A bottleneck for LNP-mediated therapeutics. Proc. Natl. Acad. Sci. USA *121*, e2307800120.

63. Zhao, M., Yang, H., Jiang, X., Zhou, W., Zhu, B., Zeng, Y., Yao, K., and Ren, C. (2008). Lipofectamine RNAiMAX: an efficient siRNA transfection reagent in human embryonic stem cells. Mol. Biotechnol. *40*, 19–26.

64. Hou, X., Zaks, T., Langer, R., and Dong, Y. (2021). Lipid nanoparticles for mRNA delivery. Nat. Rev. Mater. *6*, 1078–1094.

65. Kong, W., Wei, Y., Dong, Z., Liu, W., Zhao, J., Huang, Y., Yang, J., Wu, W., He, H., and Qi, J. (2024). Role of size, surface charge, and PEGylated lipids of lipid nanoparticles (LNPs) on intramuscular delivery of mRNA. J. Nanobiotechnol. *22*, 553.

66. Sato, H., Kato, Y., Hayasi, E., Tabata, T., Suzuki, M., Takahara, Y., and Sugiyama, Y. (2002). A novel hepatic-targeting system for therapeutic cytokines that delivers to the hepatic asialoglycoprotein receptor, but avoids receptor-mediated endocytosis. Pharm. Res. *19*, 1736–1744.

67. Breitfeld, P.P., Simmons, C.F., Jr., Strous, G.J., Geuze, H.J., and Schwartz, A.L. (1985). Cell biology of the asialoglycoprotein receptor system: a model of receptor-mediated endocytosis. Int. Rev. Cytol. *97*, 47–95.

68. Schwartz, A.L., Fridovich, S.E., and Lodish, H.F. (1982). Kinetics of internalization and recycling of the asialoglycoprotein receptor in a hepatoma cell line. J. Biol. Chem. *257*, 4230–4237.

69. Dowdy, S.F., Setten, R.L., Cui, X.S., and Jadhav, S.G. (2022). Delivery of RNA Therapeutics: The Great Endosomal Escape! Nucl. Acid. Ther. *32*, 361–368.

70. Livak, K.J., and Schmittgen, T.D. (2001). Analysis of relative gene expression data using real-time quantitative PCR and the 2(-Delta Delta C(T)) Method. Methods *25*, 402–408.

71. Chen, C.Y.A., Ezzeddine, N., and Shyu, A.B. (2008). Messenger RNA half-life measurements in mammalian cells. Methods Enzymol. *448*, 335–357.

72. Elmokadem, A., Riggs, M.M., and Baron, K.T. (2019). Quantitative Systems Pharmacology and Physiologically-Based Pharmacokinetic Modeling With mrgsolve: A Hands-On Tutorial. CPT Pharmacometrics Syst. Pharmacol. *8*, 883–893.

73. Zhang, X.Y., Trame, M.N., Lesko, L.J., and Schmidt, S. (2015). Sobol Sensitivity Analysis: A Tool to Guide the Development and Evaluation of Systems Pharmacology Models. CPT Pharmacometrics Syst. Pharmacol. *4*, 69–79.

74. Marino, S., Hogue, I.B., Ray, C.J., and Kirschner, D.E. (2008). A methodology for performing global uncertainty and sensitivity analysis in systems biology. J. Theor. Biol. *254*, 178–196.